VII International Conference on Particle-Based Methods
PARTICLES 2021
P. Wriggers, M. Bischoff, E. Oñate, M. Bischoff, A. Düster & T. Zohdi (Eds)

DISCRETE ELEMENT METHOD TO SIMULATE INTERFACE DELAMINATION AND FRACTURE OF PLASMA-SPRAYED THERMAL BARRIER COATING

W. LECLERC[1], N. FERGUEN[2], E-S. LAMINI[3], Y. MEBDOUA[2] AND M. GUESSASMA[1]

[1] Laboratoire des Technologies Innovantes (LTI, UR-UPJV 3899)
Université de Picardie Jules Verne (UPJV)
48 rue dOstende, 02100 Saint-Quentin, France
e-mail: willy.leclerc@u-picardie.fr, lti-picardie.fr/theme-mim/

[2] Centre de Développement des Technologies Avancées (CDTA)
Equipe Projection Thermique (DMIL)
Cité 20 août 1956 Baba Hassen, Alger, Algérie
e-mail: nferguen@cdta.dz, www.cdta.dz

[3] Laboratoire de REcherche opérationnelle, de Combinatoire, d'Informatique Théorique et de méthodes Stochastiques (RECITS)
Université des Sciences et de la Technologie Houari Boumédiène (USTHB)
BP 32, El Alia 16111, Bab Ezzouar, Alger, Algérie
e-mail elsedik.lamini@usthb.edu.dz

Key words: Thermal barrier coating, interface delamination, fracture, DEM, CZM

Abstract. This paper aims at investigating the potential and benefits of the Discrete Element Method (DEM) to predict failure mechanisms leading to interface delamination and fracture in air plasma sprayed Thermal Barrier Coating (TBC) systems. A hybrid lattice-particle approach is proposed to predict residual stress fields due to Coefficient of Thermal Expansion (CTE) mismatch and combined with a mixed-mode Cohesive Zone Model (CZM) to simulate interface delamination during the cooling-down phase. Numerical calculations are first performed using a unit cell model with a perfectly sinusoidal interface profile, which comes from other contributions, in order to attest the suitability of the proposed DEM-based approach for that purpose. The case of a real microstructure is then discussed via an image processing based model which underlines the effect of porosity and surface roughness on the failure mechanism.

1 INTRODUCTION

TBC systems are largely employed in gas turbines and jet engines for protecting metallic components from severe thermal conditions, prolonging their lifetime and improving their efficiency. Typically, they are composed of a ceramic Top-Coat (TC) for thermal insulation, an intermediate metallic Bond-Coat (BC) layer located between a superalloy substrate and TC, and an oxidation-resistant layer called Thermally Grown Oxide (TGO)

which develops by the diffusion of aluminum at high temperature from the BC [1]. Predicting interface delamination and failure of TBC under thermo-mechanical loading is quite complex due to severity of thermal conditions and intrinsic multilayer nature which inevitably generate residual stresses [2]. Indeed, several parameters and phenomena lead to premature TBC failure reducing consequently their operating lifetime. Among these factors, thermal expansion mismatch [3], oxidation [4], interface roughness [2] and continuously changing compositions and properties of the TBC system [5] play a major role and must be taken into account for prediction purposes. Besides, TBC fracture mechanisms also depend on TC deposition technique which impacts on microstructure morphology. Thus, Atmospheric Plasma Spray (APS) coatings are characterised by an intricate lamellar structure with interconnected pore network.

Due to the complexity of physical phenomena arising in TBC under operating conditions, numerical modelling turns out to be a relevant tool to simulate failure mechanisms, and predict and optimise their lifetime duration. In literature, Finite Element (FE) based approaches are widely used for that purpose. Thus, among other works, Aktaa et al. [2] took benefit of a modified crack closure integral method to simulate residual stresses and fracture mechanisms in a TBC system. Baeker [6] modelled TC/TGO interface delamination and investigated its influence on the out-of-plane stresses. Cen et al. [7] considered a unit cell with a sinusoidal interface profile in which TGO growth is taken into account and a Cohesive Zone Model (CZM) is introduced to simulate crack propagation along BC/TGO interface. Song et al. [8] used the same concept to study effects of different thermal cycle loadings on cracking behavior of APS coatings, and Wei et al. [4] simulated crack growth in the TC layer using the Virtual Crack Closure Technique (VCCT). Nevertheless, the failure behavior of TBC systems and more specifically of APS coatings is strongly influenced by their microstructure which is characterised by the presence of pores at the TC/BC interface [9] and crack growth between lamellae [4, 10]. This induces complex failure phenomena as multiple crack development and crack coalescence which are not easily treated in FE simulations.

In the present work, we aim at investigating the potential of DEM to investigate mechanisms leading to interface delamination and fracture in TBC. Originally developed to model granular materials, DEM was adapted to simulate continuous media using cohesive beam elements [11]. Thus, it turned into a promising approach to simulate complex fracture phenomena arising in homogeneous or heterogeneous materials under mechanical or thermo-mechanical conditions [12, 13]. In the present contribution, we take benefit of MULTICOR2D++ software developed at LTI laboratory to study a ceramic-metal multilayer constituted of a plasma-sprayed ceramic TC and a Ni alloy BC. Emphasis is first placed on thermo-mechanical stresses arising in TBC due to CTE mismatch. Effects of roughness are discussed using a unit cell model in which the TGO layer has a sinusoidal profile. In a second step, interface delamination is investigated using a mixed-mode CZM under mixed-mode conditions. Finally, similar simulations are performed on a realistic sample using a microstructure built by image processing. Such a model takes into account defects as preexistent pores and cracks and an irregular TC/BC interface. This contribu-

tion is organised as follows. Section 2 presents the DEM-based simulation approach and provides information on the implementation of mixed-mode CZM. Section 3 is devoted to numerical results obtained using a unit cell model based on a sinusoidal interface profile in terms of residual stresses and BC/TGO interfacial debonding. Section 4 adresses the interfacial delamination within a real TBC microstructure reproduced by image processing. Conclusions and prospects are finally provided in Section 5.

2 DEM-BASED SIMULATION APPROACH

2.1 Hybrid lattice-particle model

In the present work, we consider a hybrid lattice-particle model which allows for simulating a continuous medium using a random network of cohesive beam elements [11, 12]. In such a paradigm, an Equivalent Continuous Domain (ECD) is defined using a dense particulate system composed of disks in point contact in which a cohesive beam element is introduced between each pair of particles in contact. Thus, this concept provides a two-scale description of the matter where mass and inertia properties are provided by particles and macroscopic mechanical ones depend on a set of microscopic geometrical and physical parameters associated to each beam element. The micro-macro relation is closely related to intrinsic parameters of the random particulate system, as the cardinal number, the volume fraction of particles or the potential polydispersity of disks. Thus, an accurate control of these features during the generation process gives the possibility to target desired macroscopic mechanical properties via calibration results. For information purposes, in present studies, our simulations lie on the well-established framework given by the concept of Random Close Packing (RCP) which characterises itself by a cardinal number of 4.6 and a volume fraction of 0.85. Besides, a small polydispersity based on a Gaussian model with a coefficient of variation equal to 0.3 is also introduced to ensure the random behaviour of the particulate system.

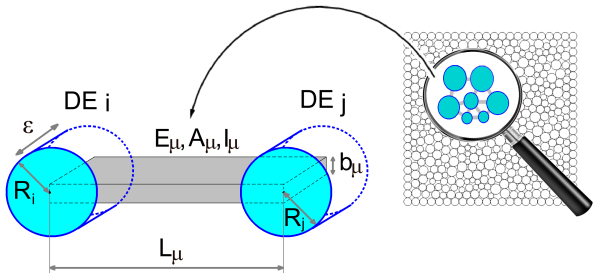

Figure 1: Cohesive beam model

Classical Euler-Bernoulli beam elements for which accurate calibration curves were established in some of our previous articles are handled in the present contribution. As depicted on Figure 1, these are described by a set of parameters: a beam length $L_\mu \approx R_i + R_j$ where R_i and R_j are the radii of both particles i and j in contact, a rectangular section A_μ, a quadratic moment I_μ and a microscopic Young's modulus E_μ. A_μ itself depends on the width of the beam b_μ and the thickness of the system ε which has no effect on mechanical simulations and is arbitrarily set to 1 for convenience, so that $A_\mu = b_\mu$. Thus, under such

an assumption, A_μ and I_μ can be directly related to R_i and R_j as follows:

$$A_\mu = r_\mu (R_i + R_j) \qquad I_\mu = \frac{A_\mu^3}{12} = \frac{r_\mu^3}{12} (R_i + R_j)^3 \tag{1}$$

where $r_\mu > 0$ can be described as a dimensionless width of the beam element. Note that, according to Haddad et al. [11], the macroscopic mechanical behaviour is poorly affected by L_μ for dense particulate systems composed of more than 7,000 particles. Thus, the set of relevant microscopic parameters can be reduced to E_μ and r_μ ones. More precisely, the 3-component generalised force vector associated to each cohesive beam element includes normal and tangential components able to counteract the relative displacement of particles, and a moment term in opposition to bending effects. Their expressions depend on E_μ and r_μ microscopic parameters and derive from a 3-by-3 matrix system provided in previous contributions [11, 12]. By applying Newton's second law, the motion of each particle is computed over the time using an explicit velocity Verlet scheme which is well-adapted for large-scale discrete simulations.

2.2 Mechanical behaviour of materials

The relation between microscopic parameters E_μ and r_μ, and the elastic coefficients E_M and ν_M of the targeted continuous domain is a priori unknown. That is why, a calibration process is typically set up to correlate microscopic and macroscopic coefficients using polynomial functions P and Q as follows:

$$r_\mu = P(\nu_M) \qquad E_\mu = Q(r_\mu) E_M \tag{2}$$

Thus, r_μ is first deduced from ν_M, and E_μ is then determined as function of r_μ and E_M. Note that, in the present work, P and Q functions derive from previous investigations led using specific tensile tests [11]. In the present contribution, we aim at modelling a TBC which is typically composed of 4 different constituents, namely the substrate, the BC, the TGO layer and the TC. Nevertheless, based on preliminary studies, we deliberately ignore the substrate since it poorly affects the stress field level and the delamination process. Besides, we limit our studies to the cooling-down step so that the TGO growth arising during the dwelling step due to the oxidation of the BC is not taken into account. Finally, all constituents are supposed homogeneous, isotropic and elastic with temperature-dependent properties. In such a framework, the continuous medium is heterogeneous and microscopic parameters have to be independently identified for each constituent. Table 1 provides macroscopic properties for TC, TGO and BC layers as well as corresponding microscopic coefficients. Material data comes from the works of Cen et al. [7] and correspond to a NiCoCrAlY BC and a yttria partially stabilized zirconia TC.

2.3 Thermal loading and expansion

Investigations are limited to the sole cooling-down step and temperature field is supposed homogeneous in space over the time. The model is cooled from an initial temperature of 1100°C to a final one of 25°C in 300s using a linear ramp. All constituents are sensitive

T(°C)	TC			TGO			BC		
	$\alpha(10^{-6}/°C)$	E_M/E_μ(GPa)	ν_M/r_μ	$\alpha(10^{-6}/°C)$	E_M/E_μ(GPa)	ν_M/r_μ	$\alpha(10^{-6}/°C)$	E_M/E_μ(GPa)	ν_M/r_μ
25	9.68	17.5/29.8	0.2/0.63	5.1	380/1060.2	0.27/0.45	-	183/510.6	0.27/0.45
100	-	-/-	0.2/0.63	-	-/-	0.27/0.45	10.34	-/-	0.27/0.45
200	9.7	-/-	0.2/0.63	-	-/-	0.27/0.45	11.3	-/-	0.27/0.45
400	-	-/-	0.2/0.63	-	-/-	0.27/0.45	12.5	152/424.1	0.27/0.45
600	-	-/-	0.2/0.63	-	353/984.9	0.27/0.45	-	-/-	0.27/0.45
700	9.88	-/-	0.2/0.63	-	-/-	0.27/0.45	-	-/-	0.27/0.45
800	-	-/-	0.2/0.63	-	338/943	0.27/0.45	14.3	109/304.1	0.27/0.45
900	-	12.4/21.1	0.2/0.63	-	-/-	0.27/0.45	16	-/-	0.27/0.45
1000	10.34	-/-	0.2/0.63	9.8	312/870.5	0.27/0.45	-	-/-	0.27/0.45

Table 1: Temp.-dependent CTE, Young's moduli and Poisson ratios of TC, TGO and BC

to thermal conditions and exposed to a thermal shrinkage according to an isotropic and temperature-dependent CTE provided in Table 1. In the DE model, thermal shrinkage (or expansion) is taken into account by reducing (or enlarging) the initial beam length $L_\mu(T_{init})$ as follows:

$$L_\mu(T) = L_\mu(T_{init})(1 + \alpha(T - T_{init})) \tag{3}$$

Note that CTE at the scale of the elementary contact is equal to macroscopic one α so that no calibration is required.

2.4 Mixed-mode cohesive zone model

TGO/BC interface delamination is modelled using cohesive zone elements. CTE mismatch during the thermal loading induces local shear and tensile/compressive stresses which can lead to the interfacial delamination during the cooling-down step. Due to the competition between tensile and shear stresses as well as the potential complexity of the TBC microstructure, we consider a mixed-mode delamination model based on a linear elastic response before damage and an exponential softening after damage [12, 14]. In the present work, the damage onset is controlled by the following criterion:

$$\left(\frac{U_n}{U_n^c}\right)^2 + \left(\frac{U_s}{U_s^c}\right)^2 = 1 \tag{4}$$

where U_n, U_s, U_n^c and U_s^c are the normal and tangential displacements and their critical counterparts. U_n^c and U_s^c are defined as function of critical energy release rates G_I^c and G_{II}^c as follows:

$$U_n^c = \sqrt{\frac{2AG_I^c}{5K_n^o}} = N/K_n^o \qquad U_s^c = \sqrt{\frac{2AG_{II}^c}{5K_s^o}} = S/K_s^o \tag{5}$$

where K_n^o and K_s^o are initial normal and tangential stiffnesses which are equal to the ones of beam elements, A is the contact area which is set to the average cross-section of cohesive beam elements in the present work, and N, S are the critical normal and shear forces. Let U_e be the effective displacement which depends on U_n and U_s:

$$U_e = \sqrt{U_n^2 + U_s^2} \tag{6}$$

and η be a coupling parameter which reads:

$$\eta = \begin{cases} \frac{U_s}{U_n} & \text{if } U_n > 0 \\ \\ 0 & \text{if } U_n \leq 0 \end{cases} \tag{7}$$

Then, after injecting Equation 4 in 6, we can define a critical effective displacement U_e^c

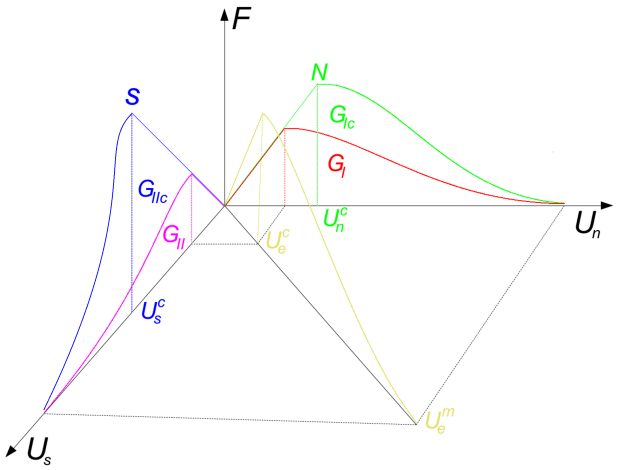

Figure 2: Mixed-mode exponential softening law

(see Figure 2) related to the damage initiation which expresses as function of U_n^c and U_s^c as follows:

$$U_e^c = \begin{cases} U_n^c U_s^c \sqrt{\dfrac{1+\eta^2}{(U_n^c)^2 + (\eta U_s^c)^2}} & \text{if } U_n > 0 \\ \\ U_s^c & \text{if } U_n \leq 0 \end{cases} \tag{8}$$

Finally, the constitutive mechanical response for mixed-mode fracture is defined as function of a damage parameter D which reads:

$$D = \begin{cases} 0 & \text{if } U_e \leq U_e^c \\ \\ 1 - e^{-\left(\frac{U_e - U_e^c}{U_e^c}\right)} & \text{if } U_e^c < U_e \leq U_e^m \\ \\ 1 & \text{if } U_e > U_e^m \end{cases} \tag{9}$$

where U_e^m is a threshold effective displacement beyond which we suppose that the cohesive bond is fully debonded. U_e^m is set to 15 times U_e^c in all numerical simulations discussed in this contribution. From a practical standpoint, normal and tangential stiffnesses K_n and K_s related to cohesive zone elements are defined during the delamination process as function of K_n^o, K_s^o and D:

$$K_n = K_n^o(1-D) \qquad K_s = K_s^o(1-D) \tag{10}$$

3 VALIDATION STUDIES USING A UNIT CELL MODEL

3.1 Unit cell model

For validation purposes, we first model the TBC system using a unit cell with a sinusoidal interface profile of wavelength and amplitude respectively equal to 12 and 5 μm. Dimensions are provided in Figure 3 and mostly come from Cen et al.'s work [7] and Baekers's contributions [6]. The periodicity of this model allows us to reduce the representative cell to a half-period as also depicted in Figure 3. Symmetry boundary conditions are imposed on the bottom edge of the unit cell model to take this into account. Note that, in the present study, we limit our simulations to a 3-phase model composed of BC, TGO and TC layers. Indeed, preliminary studies exhibited that the substrate poorly affects the stress level and the delamination process.

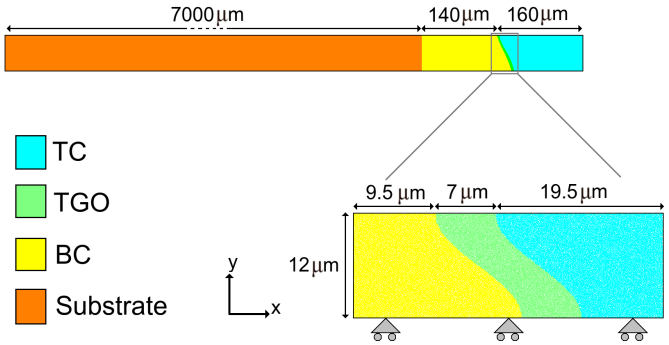

Figure 3: Unit cell model of thermal barrier coating system

3.2 Stress fields

Stress fields are determined using symmetrised Zhou's formulation of stress tensor [15]:

$$\overline{\overline{\sigma}}_{\mathrm{I}} = \frac{1}{2|\Omega_{\mathrm{I}}|} \sum_{i \subset \Omega_{\mathrm{I}}} \sum_{j=1}^{Z_i} \frac{1}{2} \left(\mathbf{l}_{ij} \otimes \mathbf{f}_{ij} + \mathbf{f}_{ij} \otimes \mathbf{l}_{ij} \right) \tag{11}$$

where Z_i is the local cardinal number of DE i, $\mathbf{f}_{ij}$ is the interparticle force vector exerted by DE j on DE i, $\mathbf{l}_{ij}$ is the relative position vector between DE i and j and Ω_{I} is an area surrounding a given particle I. In present studies, based on recent works of Moukadiri et al. [16], this latter is set as a disk (or a part of disk when DE I is located close to the domain boundaries or an interface between two or more layers) of same center than DE I and radius $\mathrm{R}_{\Omega_{\mathrm{I}}} = \mathrm{hR}_{\mathrm{I}}$. h is a multiplier coefficient also called the halo size of DE I which depends on the particle density and the model configuration, and requires as such prior studies. Thus, in a first step, before all investigations, we aim at evaluating the suitable particle density in the particulate system as well as h parameter. Figure 4 depicts the evolution of minimum and maximum σ_{xx} stress as function of the density of particles for a number of DE in the 1800-45000 interval. For information purposes, the maximum stress is located in the peak region of the BC layer and the minimum one is located in the valley region of the TGO layer. Numerical simulations exhibit a kind of convergence towards minimum and maximum values of about -800 and 600 MPa which are only reached for a number of particles higher than 15000/20000 particles. Minimum and maximum σ_{xx}

stress are then determined as function of the halo size for a number of particles set to 22000 DE. Again, a near convergence is observed which is reached for a miminum halo size of 5. Thus, based on these preliminary studies and for what follows, all discrete simulations performed on the unit cell model use a halo size of 5 and a number of 22000 particles. In a second step, we aim at determining σ_{xx} and σ_{yy} stress fields within the

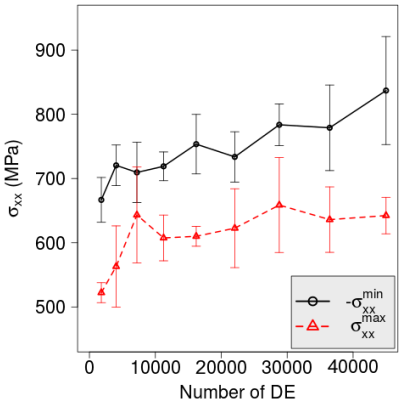

Figure 4: Evolution of minimum and maximum σ_{xx} stress as function of DE density

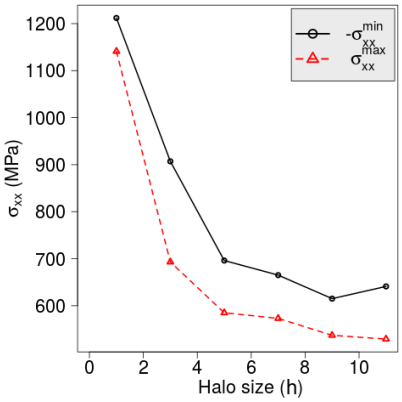

Figure 5: Evolution of minimum and maximum σ_{xx} stress as function of the halo size

TBC system. Figure 6 depicts σ_{xx} stress field at the end of the cooling-down step. From a qualitative standpoint, results are quite similar to those obtained by Cen et al. [7] with maximum stresses located in the peak region of the BC layer and minimum ones in the valley region of the TGO layer. The maximum stress value is 585 MPa which is not far from the FE estimate of previous authors which is 735 MPa. In the case of the minimum stress, we obtain a value of -696 MPa which does not agree with Cen et al.'s prediction which is -2938 MPa. Besides, this is located in the valley region of the TGO layer near the TC/TGO interface while stress minimum provided by the present model is close to BC/TGO interface. Nevertheless, one has to keep in mind that we limit our simulations to the cooling-down step and TGO growth step is not considered in our model. Thus, in spite of stress history related to heating-up and dwelling steps of thermal cycle applied to the TBC, the stress field is assumed to be zero at the initial state of DE calculations. Besides, we limit our investigations to a perfect TGO layer with a constant thickness of 7 μm while this should be more irregular due to the heterogeneity of TGO growth. Figure 7 illustrates the distribution of σ_{yy} stress field at the same instant than σ_{xx} stress. Numerical outputs exhibit that maximum stresses are again located in the peak region of the BC layer but minimum ones are this time observed in the peak region of TGO growth close to BC/TGO Interface. Minimum and maximum σ_{yy} stresses are respectively 548 MPa and -1616 MPa, which is of same order of magnitude as that of σ_{xx} stress field. Figures 8 and 9 show σ_{xx} and σ_{yy} stress fields in the TC layer. Again, in the case of σ_{xx} stress field, results are in quite good agreement with those of Cen et al. [7] with a positive maximum stress situated in the valley region and a negative minimum one located in the peak region. Maximum and minimum σ_{xx} stress values are respectively equal to 59.9 and

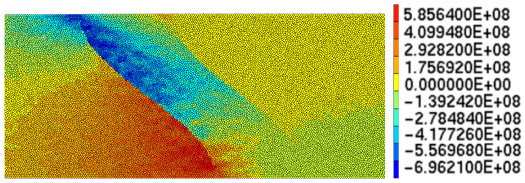

Figure 6: σ_{xx} stress field in TBC system

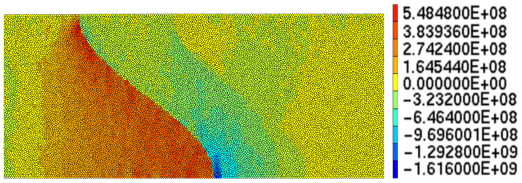

Figure 7: σ_{yy} stress field in TBC system

-36.5 MPa, which is in relative good agreement with values obtained by Cen et al. using FE simulations, namely 80 and -82 MPa. This signifies that cracks are more prone to develop in the valley region, parallelelly of TC layer surface, than the peak region which is in compressive state. Such a finding is consistent with experimental observations. In the case of σ_{yy} stress field, positive values are located in peak and valley regions of TC with a maximum value of 44.4 MPa. Negative stresses concentrate in the middle sector of TGO/TC interface with a minimum value of -36.9 MPa.

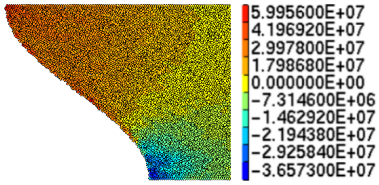

Figure 8: σ_{xx} stress field in TC layer

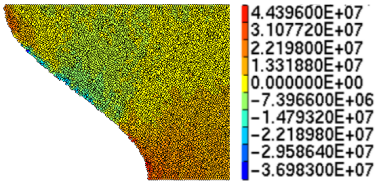

Figure 9: σ_{yy} stress field in TC layer

3.3 TGO/BC interface delamination

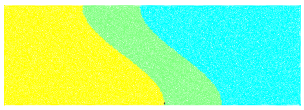

(a) ΔT= -280.53°C

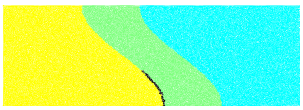

(b) ΔT= -281.21°C

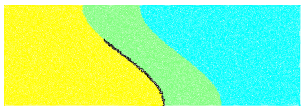

(c) ΔT= -281.91°C

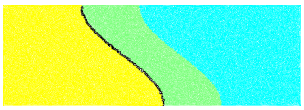

(d) ΔT= -282.36°C

Figure 10: TGO/BC interface delamination as function of thermal loading (unit cell)

TGO/BC interface delamination is modelled using the mixed-mode cohesive zone model discussed in subsection 2.4. The configuration of the unit cell model is unchanged except that no boundary condition is now considered to ensure delamination is unbiased and only related to CTE mismatch. For information purposes, the time step is set to 1.7403×10^{-7}s and the particulate system is still composed of 22,000 particles. Critical energy release rates G_I^c and G_{II}^c are deliberately set to low values of 0.2 and 0.6 N/m respectively in order to observe a complete interfacial delamination. Figures 10a, b, c and d illustrate the TGO/BC interface delamination process as function of thermal loading. Interfacial debonding starts at a temperature difference ΔT of -280.53°C at the lowest position of the peak region of TGO/BC interface. Then, delamination steadily evolves until a final temperature difference ΔT of -282.36°C for which the TGO/BC interface is fully

debonded. The corresponding process duration is 0.511s, which represents only 0.142% of the total cooling-down step duration and exhibits a relatively fast delamination process. From a qualitative standpoint, results are in agreement with FE simulations led by Cen et al. which observed the same departure point. They also agree well with Aktaa et al.'s conclusions [2] which claim that crack initiation is more prone to occur in the peak region in the case of a low roughness amplitude as studied here. Nevertheless, we must precise that delamination is potentially influenced by, among other parameters or phenomena, matrix cracking, preexistent porosity and interface discontinuities which are not taken into account in the present investigated model.

4 APPLICATION TO A REAL TBC MICROSTRUCTURE

4.1 Image processing based model

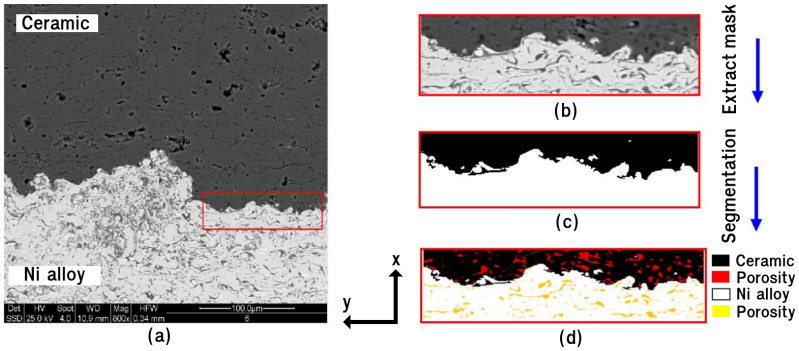

Figure 11: a) SEM image of ceramic TC sprayed onto a Ni alloy BC. b) to c) Applying mask filter for interface detection. c) to d) Segmentation process to extract microstructure

We now aim at investigating the case of a real TBC microstructure with irregular roughness and porosity. For that purpose, we consider a sample of a TBC composed of a ceramic TC sprayed on a nickel alloy BC which is very similar to the material discussed in the previous paragraph. Thus, for simplicity and comparison purposes, material data of each layer is chosen exactly the same as for the context of the unit cell problem. The numerical model is defined using a segmentation process applied to an SEM image of the targeted TBC system before thermal loading so that TGO layer is not taken into account here. From a practical standpoint, we perform a 2-step approach aiming at detecting the boundaries between TC and BC according to their gray level characteristics. Figure 11 illustrates the segmentation process to determine extrinsic microstructure features using a mask filter. The rectangle red color of Figure 11a) designates the selected rectangular sample the dimensions of which are 127mm×35mm. A mask filter is first extracted from the SEM image and applied over the whole image to detect interfaces and distinguish TC and BC layers (Figures 11b) and c)). Then, a segmentation process allows us to extract microstructure features as porosity (Figure 11b)). Thus, the final model is composed of 4 phases: TC and BC layers and porosity related to each one. From a simulation standpoint, porosity phases are recreated by removing particles from a dense particulate system composed of 25,000 particles, which enables to ensure a suitable equivalence between the

amount of removed particles and the void fraction. Note that, in the present case, cohesive zone elements are placed at TC/BC interface since TGO layer is not considered.

4.2 Interface delamination

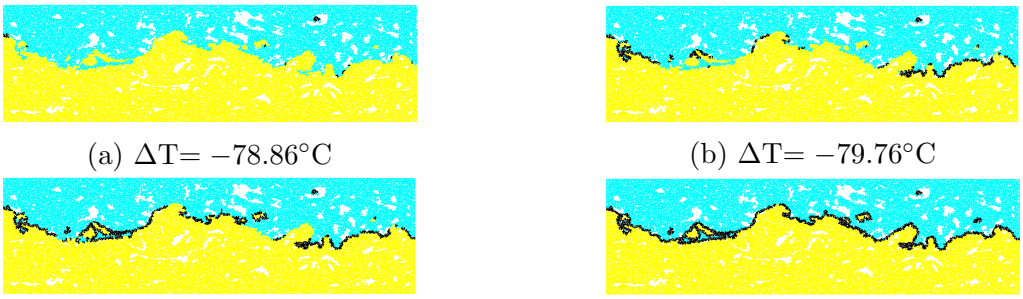

(a) ΔT= -78.86°C (b) ΔT= -79.76°C

(c) ΔT= -80.22°C (d) ΔT= -82.36°C

Figure 12: TC/BC interface delamination as function of thermal loading (realistic model)

TC/BC interface delamination is investigated using the hypotheses discussed in subsection 3.3 except that the time step is now set to 4.4793×10^{-6}s. Figures 12a, b, c and d illustrate the TC/BC interface delamination process as function of thermal loading. Results exhibit that the debonding starts at several isolated positions for ΔT= -78.86°C. Then, delamination tends to initiate in peak regions and evolves rapidly until a temperature difference ΔT= -82.35°C from which TC/BC interface is fully debonded. Thus, the delamination initiates much earlier than for the unit cell model and the process duration of 0.965s is also a little bit longer. We hypothesize that this is mainly related to the absence of TGO layer and the irregular roughness which locally generates higher stresses.

5 CONCLUSIONS AND PROSPECTS

A DEM-based approach was considered to predict residual stress fields due to CTE mismatch and combined with a mixed-mode CZM to simulate BC/TGO layer interfacial delamination in TBC systems. In a first step, studies focused on a unit cell model with a perfectly sinsusoidal TGO layer which comes from literature. Results in terms of stress fields and delamination turned out to be in good agreement with experimental observations and FE predictions discussed in other contributions. The case of a real TBC microstructure with porosity and an irregular roughness was studied in a second step using an image processing based model. Simulations exhibited that delamination is sensitive to surface roughness and tends to initiate in peak regions. In a next future, we expect to extend the proposed DEM model to a complete thermal cycling including heating-up and dwelling phases, and predict cracks propagation in TC layer.

References

[1] Evans, A.G. and Hutchinson J.W. The mechanics of coating delamination in thermal gradients. *Surf. Coat. Technol.* (2007) **201(18)**:7905–7916.

[2] Aktaa J., Sfar K. and Munz D. Assessment of TBC systems failure mechanisms using a fracture mechanics approach. *Acta Mater.* (2005) **53**:4399–4413.

[3] Traeger F., Ahrens M., Vassen R. and Stoever D. A life time model for ceramic thermal barrier coatings. *Mater. Sci. Eng. A* (2003) **358**:255–265.

[4] Wei Z-Y. and Cai H-N. Stress states and crack behavior in plasma sprayed TBCs based on a novel lamellar structure model with real interfacial morphology. *Ceram. Int.* (2019) **45(14)**:16948–16962.

[5] Padture N.P., Gell M. and Jordan E.H. Thermal barrier coatings for gas turbine engine applications. *Sci.* (2002) **296(5566)**:280–284.

[6] Baeker M. Finite element simulation of interface cracks in thermal barrier coatings. *Comput. Mater. Sci.* (2012) **64(3)**:79–83.

[7] Cen L., Qin W.Y. and Yu Q.M. Analysis of interface delamination in thermal barrier coating system with axisymmetric structure based on corresponding normal and tangential stresses. *Surf. Coat. Technol.* (2019) **358**:785–795.

[8] Song J., Li S., Yang X., Qi H. and Shi D. Numerical investigation on the cracking behaviors of thermal barrier coating system under different thermal cycle loading waveforms. *Surf. Coat. Technol.* (2018) **349**:166–176.

[9] Bialas M. Finite element analysis of stress distribution in thermal barrier coatings. *Surf. Coat. Technol.* (2008) **202**:6002–6010.

[10] Krishnasamy J., Sathiskumar A.P., Turteltaub S. and van der Zwaag S. Numerical investigation into th effect of splat pores on the thermal fracture of air plasma-sprayed thermal barrier coatings. *J. Therm. Spray Tech.* (2019) **28**:1881–1892.

[11] Haddad H., Leclerc W., Guessasma M., Pélegris C., Ferguen N. and Bellenger E. Application of DEM to predict the elastic behavior of particulate composite materials. *Granul. Matter* (2015) **17(4)**:459–473.

[12] Leclerc W., Haddad H. and Guessasma M. On the suitability of a discrete element method to simulate cracks initiation and propagation in heterogeneous media. *Int. J. Solids Struct.* (2017) **108**:98–114.

[13] Ferguen N., Mebdoua-Lahmar Y., Lahmar H., Leclerc W. and Guessasma M. DEM model for simulation of crack propagation in plasma-sprayed alumina coatings. *Surf. Coat. Technol.* (2019) **371(15)**:287–297.

[14] Ammar A., Leclerc W., Guessasma M. and Haddar N. Discrete element approach to simulate debonding process in 3D short glass fibre composite materials: Application to PA6/GF30. *Compos. Struct.* (2021) **270(2)**:114035.

[15] Zhou M., A new look at the atomic level virial stress: on continuum molecular system equivalence. Proceedings of the Royal Society of London. *Math. Phys. Eng. Sci.* (2003) **2037**:2347–2392.

[16] Moukadiri D., Leclerc W., Khellil K., Aboura Z., Guessasma M., Bellenger E. and Druesne F. Halo approach to evaluate the stress distribution in 3D Discrete Element Method simulation : Validation and application to flax/bio based epoxy composite. *Model. Simul. Mater. Sci. Eng.* (2019) **27(6)**:065005.